HHS Public Access

Author manuscript

Biochem J. Author manuscript; available in PMC 2020 January 29.

Published in final edited form as:

Biochem J. 2013 April 01; 451(1): 33–44. doi:10.1042/BJ20121307.

Identification of the activator-binding residues in the second cysteine-rich regulatory domain of protein kinase Cθ (PKCθ)

Ghazi M. Rahman[*], **Sreejesh Shanker**[†], **Nancy E. Lewin**[‡], **Noemi Kedei**[‡], **Colin S. Hill**[‡], **B. V. Venkataram Prasad**[†,§], **Peter M. Blumberg**[‡], **Joydip Das**[*,1]

[*]Department of Pharmacological & Pharmaceutical Sciences, College of Pharmacy, University of Houston, Houston, TX 77204, U.S.A.

[†]Verna Marrs Mclean Department of Biochemistry and Molecular Biology, Baylor College of Medicine, Houston, TX 77030, U.S.A.

[‡]Laboratory of Cancer Biology and Genetics, Center for Cancer Research, National Cancer Institute, Bethesda, MD 20892, U.S.A.

[§]Department of Molecular Virology and Microbiology, Baylor College of Medicine, Houston, TX 77030, U.S.A.

Abstract

PKC (protein kinase C) θ is predominantly expressed in T-cells and is critically involved in immunity. Design of PKCθ-selective molecules to manage autoimmune disorders by targeting its activator-binding C1 domain requires the knowledge of its structure and the activator-binding residues. The C1 domain consists of twin C1 domains, C1A and C1B, of which C1B plays a critical role in the membrane translocation and activation of PKCθ. In the present study we determined the crystal structure of PKCθC1B to 1.63 Å (1 Å = 0.1 nm) resolution, which showed that Trp^{253} at the rim of the activator-binding pocket was orientated towards the membrane, whereas in PKCδC1B the homologous tryptophan residue was orientated away from the membrane. This particular orientation of Trp^{253} affects the size of the activator-binding pocket and the membrane affinity. To further probe the structural constraints on activator-binding, five residues lining the activator-binding site were mutated (Y239A, T243A, W253G, L255G and Q258G) and the binding affinities of the PKCθC1B mutants were measured. These mutants showed reduced binding affinities for phorbol ester [PDBu (phorbol 12,13-dibutyrate)] and diacylglycerol [DOG (*sn*-1,2-dioctanoylglycerol), SAG (*sn*-1-stearoyl 2-arachidonyl glycerol)]. All five full-length PKCθ mutants exhibited reduced phorbol-ester-induced membrane translocation compared with the wild-type. These results provide insights into the PKCθ activator-binding domain, which will aid in future design of PKCθ-selective molecules.

[1]To whom correspondence should be addressed (jdas@uh.edu).

AUTHOR CONTRIBUTION

Joydip Das designed the research. Ghazi Rahman, Sreejesh Shanker, Nancy Lewin, Noemi Kedei and Colin Hill performed the research. Ghazi Rahman, Joydip Das, Sreejesh Shanker, Nancy Lewin, Noemi Kedei, Colin Hill, Venkataram Prasad and Peter Blumberg analysed the results. Joydip Das, Ghazi Rahman, Sreejesh Shanker and Peter Blumberg wrote the paper.

The structural co-ordinates for PKCθC1B have been submitted in the Protein Data Bank under accession code 4FKD.

Keywords

activator-binding residues; diacylglycerol; crystal structure; membrane translocation; phorbol ester; phospholipid; protein kinase C; tryptophan

INTRODUCTION

PKC (protein kinase C) θ is a serine/threonine kinase [1]. In humans it is encoded by the *PRKCQ* gene and is highly expressed in T-cells and thymocytes [2]. PKCθ plays a crucial role in T-cell activation and is critically involved in immunity. PKCθ is linked to the TCR (T-cell receptor) signalling complex, which in turn activates transcription factors such as NF-κB (nuclear factor κB) and AP-1 (activator protein 1), mediating immune responses [3,4]. An overactive immune system is responsible for different immunity-related complications such as arthritis [5], asthma [6], multiple sclerosis [7,8], Type 1 diabetes [9] etc. PKCθ-knockout mice were found to be protected from asthma or arthritis in response to antigen challenge, indicating the importance of PKCθ in the pathway of downstream immune responses [5,7,10,11].

In the stepwise activation process of T-cells, macrophages first respond to APCs (antigen-presenting cells), which present the antigens derived from bacteria, viruses, parasites, prions etc. The antigenic proteins generated by the digestion of APC debris bind to the MHC present on the macrophage cell surface. T-cells are then activated by the stable interaction of TCR molecules with the MHC-bound antigenic proteins. Activated TCR molecules, upon clustering at the immunological synapse, trigger the activation of PLCγ1 (phospholipase Cγ1) at the T-cell membrane, leading to formation of DAG (diacylglycerol) and Ins(1,4,5)P_3 from PtdIns(4,5)P_2 [12]. DAG binds to PKCθ, which results in the translocation of active PKCθ to the immunological synapse. Activated PKCθ at the immunological synapse, in turn, mediates the activation of the downstream transcription factors associated with the immune response, such as NF-κB, NFAT (nuclear factor of activated T-cells) and AP-1, and production of interleukin-2 [3,4,13].

The PKC superfamily comprises 11 subtypes, which have been categorized as typical and atypical. Typical C1 domains bind the endogenous activator DAG or the ultra-potent phorbol esters, whereas atypical ones are insensitive to them. The typical PKCs are further divided into the conventional (α, βI, βII and γ) and novel (δ, ε, θ and η) classes, each having four primary domains. The N-terminal regulatory region has C1 and C2 domains, whereas the highly homologous C-terminal kinase region consists of C3 and C4 domains (Supplementary Figure S1 at http://www.biochemj.org/bj/451/bj4510033add.htm) [14]. DAG is sufficient to activate the novel PKCs, whereas the conventional PKCs additionally require Ca^{2+} for their activation. DAG is a lipid second messenger that selectively interacts with proteins containing a C1 domain and induces their translocation to discrete subcellular compartments such as the plasma membrane, Golgi etc. In both conventional and novel PKCs, the DAG/phorbol-ester-responsive C1 domain consists of a tandem repeat of highly conserved cysteine-rich zinc-finger subdomains known as C1A and C1B. These subdomains

show significant differences in their binding affinities for phorbol esters and DAG [15]. Atypical PKCs (ζ and ι/λ) have a single non-DAG-binding C1 domain [14,16,17].

Several PKC isoforms (α, β1, δ, ε, η, θ and ζ) are expressed in T-cells, but only PKCθ stably translocates to the immunological synapse. Other PKCs translocate to other regions of the plasma membrane. Selective inhibition of PKCθ, therefore, could be an attractive approach in the management of a hyperactive immune system, leading to suppression of related disorders [18].

Design of PKCθ inhibitors targeting the kinase region faces a major challenge in achieving selectivity because there is a high degree of homology in the kinase region among the more than 500 kinases in the human genome [8,19]. On the other hand, there are fewer C1 domains (less than 30 phorbol ester/DAG-responsive C1 domains). Furthermore, PKCθ is unique among the conventional and novel PKC isoforms in that PKCθC1B is the only C1B subdomain that binds to DAG with higher affinity than the C1A subdomain [20]. Likewise, PKCθC1B plays the predominant role in the membrane translocation and activation process of PKCθ [21].

In the present study, we report the crystal structure of the PKCθC1B subdomain at 1.63 Å (1 Å = 0.1 nm) resolution. To identify the activator-binding residues, we performed virtual molecular docking to the PKCθC1B domain of a small library of DAG and phorbol ester analogues using the PKCθC1B crystal structure. This docking predicted that five residues, Tyr^{239}, Thr^{243}, Trp^{253}, Leu^{255} and Gln^{258}, were particularly important for ligand binding. A sequence alignment of PKCθC1B with PKCδC1B showed that all of these five residues were present in the homologous activator-binding region of PKCδC1B [22]. We confirmed that mutation of PKCθC1B in these residues, specifically Y239A, T243A, W253G, L255G and Q258G, reduced affinity for both phorbol ester and DAG. Likewise, in the full-length PKCθ, these mutations caused significantly reduced membrane translocation by phorbol ester treatment.

EXPERIMENTAL

Chemicals, reagents and antibodies

Escherichia coli BL21-Gold (DE3) competent cells were from Stratagene. SOC (super optimal culture) medium, LB (Luria-Bertani) broth medium and TB (terrific broth) medium were from Invitrogen. Glycerol, IPTG (isopropyl β-D-thiogalactopyranoside), zinc sulphate, ampicillin, lysozyme, Triton X-100, polyethyleneimine, sodium chloride, γ-globulins (G5009), Tween 20 and methanol were from Sigma–Aldrich. Thrombin, glutathione–Sepharose 4B and Superdex 75 prepacked columns were from GE Healthcare Biosciences. PMA and PDBu (phorbol 12,13-dibutyrate) were from LC Laboratories. DOG (*sn*-l,2-dioctanoylglycerol), SAG (*sn*-1-stearoyl 2-arachidonyl glycerol), PS (L-α-phosphatidylserine) and PC (L-α-phosphatidylcholine) were from Avanti Polar Lipids. Ammonium sulfate, poly(ethylene glycol) 6000 and BSA were from EMD Chemicals. Sapintoxin D was from Alexis Biochemicals. [20-^{3}H]PDBu was custom synthesized by PerkinElmer Life Sciences. DMEM (Dulbecco's modified Eagle's medium) high glucose, FBS (fetal bovine serum) and antibiotic/antimycotic concentrate used for the cell culture

were from Gibco. Rabbit anti-GFP (green fluorescent protein) antibody and HRP (horseradish peroxidase)-conjugated anti(rabbit IgG) antibody used for the Western blot analysis were purchased from Cell Signaling, and SuperSignal West Femto Maximum Sensitivity Substrate used for chemiluminescence was obtained from Thermo Scientific.

Expression vector construction

A bacterial expression vector of PKCθC1B with an N-terminal GST (glutathione transferase) tag was generated by subcloning the domain sequence (amino acids 232–281) from mouse PKCθ cDNA into the pGEX2TK vector (GE Healthcare Biosciences) between the restriction sites BamHI and EcoRI [23]. The GST-fused protein contained a thrombin cleavage site between GST and the C1B subdomain. A mammalian expression vector of mouse PKCθ with an EGFP (enhanced GFP) tag at the C-terminus was generated by subcloning the corresponding genes with the spacer sequence GGNSGG into the pEGFPNl vector (Addgene) between restriction sites BamHI and XhoI as described previously [24]. Dr Amnon Altman (La lolla Institute for Allergy and Immunology, La lolla, CA, U.S.A.) provided the original PKCθ full-length vector.

Generation of PKCθC1B and PKCθ mutants

The single point mutations (Y239A, T243A, W253G, L255G and Q258G) in the truncated PKCθC1B subdomain as well as in the full-length PKCθ were introduced by PCR using the QuikChange® Site-Directed Mutagenesis kit (Stratagene) [25–27]. Oligonucleotide primers were custom synthesized by Seqwright. The mutations were checked for their correct sequences using the sequencing facility at Seqwright.

Protein expression, purification and characterization

The PKCθC1B subdomain and its mutants fused with N-terminal GST were expressed in the *E. coli* strain BL21-Gold (DE3) (Stratagene). Expression and purification were performed following the methods described previously [28–30]. The purity of the proteins was checked by SDS/PAGE (15% gel). The exact molecular mass of the proteins was measured by MALDI–TOF-MS (matrix-assisted laser-desorption ionization–time-of-flight MS; Voyager DE-STR Biospectrometry Workstation; Applied Biosystems). Proteins were further characterized by their binding to SAPD (sapintoxin D; a fluorescent phorbol ester) using fluorescence spectroscopy (QuantaMaster™ 30; PTI) [31] in the absence of any added lipid.

Cell culture for Western blotting

A HEK (human embryonic kidney)-293 cell line expressing the ecdysone receptor (Invitrogen) was used to express the full-length PKCθ and its C1B subdomain mutants. The cells were cultured in plastic Petri dishes in DMEM supplemented with 10% FBS and 1% antibiotic/antimycotic solution at 37 °C in 5% CO_2 and 98% humidity. The confluent cells (90%) were transfected by adding 1 ml of unsupplemented DMEM containing 6 μg of endotoxin-free plasmid and 9 μl of Plus reagent (Invitrogen) and 9 μl of Lipofectamine™ reagent (Invitrogen) for 12 h at 37°C. The transfection medium was removed and the cells were washed with 1× PBS followed by the addition of antibiotic-free DMEM supplemented with FBS. Protein expression was induced for 48 h from the time of transfection before the

cells were ready for membrane translocation studies [21,32]. The expression of the full-length PKCθ and its mutants was detected by Western blot analysis of the cell lysate 48 h post-transfection using rabbit anti-GFP primary antibody and HRP-conjugated anti-(rabbit IgG) secondary antibody.

Crystallization, data collection and refinement

The hanging-drop vapour-diffusion method was used to grow PKCθC1B crystals. The protein was concentrated to 25 mg/ml in gel filtration buffer (50 mM Tris, 150 mM NaCl, 2 mM dithiothreitol and 50 μM $ZnSO_4$, pH 7.2) and was mixed at a 1:1 ratio of reservoir solution consisting of 0.1 M lithium acetate and 20% poly(ethylene glycol) 3350 at 20°C. Protein crystals appeared in 7–10 days. Crystals were cryo-protected using 10% glycerol in mother liquor followed by flash-freezing in liquid nitrogen [33]. Data were collected at the home source RIGAKU FR-E^+ (Rigaku) at Baylor College of Medicine (Houston, TX, U.S.A.). Data were processed using Mosflm and programs implemented in the CCP4 suite [34]. The space group of the crystal was confirmed by the program POINTLESS [35]. The initial phase problem was solved with the molecular replacement program PHASER [36] using the available structure (PDB code 1PTQ) followed by automated model building and solvent addition using ARP/wARP [37]. Further model refinement was carried out with Refmac (CCP4) [38] and COOT [39]. Final co-ordinates were deposited into the PDB under the accession code 4FKD.

Molecular docking

Three-dimensional chemical structures of DAG and phorbol ester analogues were downloaded from PubChem and were subjected to pre-dock energy minimization using the Powell method in Sybyl 8.0 (Tripos International) with an iteration of 100. These analogues were incorporated together into a single library ready to be docked into the crystal structure of PKCθC1B. A residue-based molecular docking was done in the SurflexDock module of Sybyl 8.0 using a threshold of 0.5, a bloat of 2.0 and a radius of 3 Å for the protomol generation. Protomol is the geometric constraint developed computationally where the ligands were docked. Residues Tyr^{239}, Lys^{240}, Ser^{241}, Pro^{242}, Thr^{243}, Phe^{244}, Leu^{251}, Leu^{252}, Trp^{253}, Gly^{254}, Leu^{255} and Glu^{258} were used to generate the protomol. These residues were selected by comparison with the phorbol ester binding site in PKCδC1B. Ring flexibility, soft grid treatment, pre-dock and post-dock energy minimization were also applied for the docking procedure. A high total score value represents better fitting. The surface area and the volume of the activator-binding pocket of C1B domains were measured using the program CASTp [40].

[^{3}H]PDBu binding assay

Binding of PDBu, DOG and SAG to PKCθC1B and its mutants was measured using the poly(ethylene glycol) precipitation assay method as described previously [41]. K_d values were determined by fitting the data into a two-component model of saturable receptor binding plus linear non-specific binding [41]. Binding affinities of DOG and SAG to PKCθC1B and its mutants were determined by competition of [^{3}H]PDBu binding using the above conditions, but with [^{3}H]PDBu at 2–5-fold the concentration of the K_d for each mutant and with a series of concentrations of DOG or SAG (1–100000 nM). The DOG or

SAG was dissolved in chloroform and added to the phospholipid. The lipid was then dried down, buffer was added, and the mixture was sonicated and finally added to the assay. Sonication was performed with a Model XL2020 sonicator (Misonix) at room temperature with four pulses of 5 s using a microtip sonicator probe at 5% power. For analysis of the dependence on the phospholipid composition, total phospholipid was maintained at 100 μg/ml. The final concentration of PS was varied from 0 to 100% with the remainder as PC [41].

Membrane translocation of PKCθ

HEK-293 cells expressing full-length PKCθ and its C1B mutants were treated with PMA or DOG for 2 h as described previously [42]. Harvested cells were then washed with ice-cold PBS and were resuspended in lysis buffer (20 mM Tris, pH 7.4) containing protease inhibitor cocktail. Cells were lysed by multiple cycles of extrusion from and re-uptake by a 1 ml of insulin syringe with a 16 gauge needle. The cell lysate was then subjected to ultracentrifugation (76000 rev./min; Beckman TLA 120.2 rotor) for 1 h at 4 °C. The supernatant was designated as the cytosolic fraction. The pellet was then resuspended again in lysis buffer with protease inhibitor and 1% Triton X-100 and kept on ice for 1 h. The mixture was sonicated three times with a 5 s pulse using a Branson digital sonifier model 250. The mixture was then further subjected to ultracentrifugation (76000 rev./min; Beckman TLA 120.2 rotor) for 1 h at 4°C. This supernatant was designated as the membrane fraction [43]. Western blot analysis of the cell fractions was performed as described previously [44]. The proteins were transferred to a nitrocellulose (0.45 μm) membrane and were detected using an anti-EGFP primary antibody (1:5000 dilution) followed by treatment with an HRP-linked secondary antibody (1:5000 dilution) for visualization. An enhanced chemiluminescence detection system from Thermo Scientific was used to visualize the labelled protein bands. The relative intensities of the protein bands were calculated using an AlphaImager from Alpha Innotech [42].

Confocal analysis of PKCθ wild-type and different mutants

Confocal analysis of the different GFP–PKCθ constructs transfected into the LNCaP prostate cancer cell line and quantification of the images was performed as described in [45].

Statistical analysis

The significance of the data obtained (for both PKCθ wild-type and its C1B mutants) from the activator-induced membrane translocation study was assessed using an unpaired two-tail *t* test. $P < 0.05$ was considered significant.

RESULTS

Expression, purification and characterization of PKCθC1B and its mutants

The C1B domains of PKCθ and its mutants were expressed as fusion proteins with an N-terminal GST tag in *E. coli*. SDS/PAGE of the whole-cell lysates confirmed high levels of expression of all of the GST-fused C1B proteins. After initial affinity purification through glutathione–Sepharose 4B columns and subsequent cleavage of the GST tag, the proteins were further purified by ammonium sulfate precipitation and gel-filtration chromatography.

Purified PKCθC1B and the mutants were obtained in good yields. For PKCθC1B, Y239A, T243A, W253G, L255G and Q258G, the yields were 9.6, 3.6, 2.4, 15.4, 4.3 and 3.9 mg/l of TB medium respectively. Purified proteins were thoroughly characterized by SDS/PAGE, MALDI–TOF-MS and phorbol ester binding. All of the proteins showed a single symmetrical peak upon elution from the Superdex-75 column with retention times corresponding to their Stokes radii, indicating the purity as well as the proper folding of the proteins (illustrated for wild-type PKCθC1B in Supplementary Figure S2A at http://www.biochemj.org/bj/45l/bj4510033add.htm; results not shown for the mutants). Using SDS/PAGE, all the proteins showed a single sharp band near 7 kDa, indicating the purity of the proteins (Supplementary Figure S2B). The molecular masses of the proteins were further confirmed by MAFDI–TOF-MS (illustrated for wild-type PKCθC1B in Supplementary Figure S2C; results not shown for the mutants). For PKCθC1B, Y239A, T243A, W253G, L255G and Q258G, the molecular masses were found to be 7333, 7245, 7305, 7210, 7281 and 7272 Da respectively with an accuracy of ±0.04%.

Expression and characterization of PKCθ and its C1B subdomain mutants in HEK-293 cells

Western blot analysis of the whole-cell lysate of HEK-293 cells transiently transfected with plasmids encoding PKCθ and its various mutants showed a band near 100 kDa, confirming the expression of the full-length PKCθ and its C1B subdomain mutants (results not shown).

Crystal structure of PKCθC1B

The diamond-shaped crystals of PKCθC1B with an average dimension of 0.2 mm×0.1 mm×0.05 mm were obtained as described in the Experimental section. The crystals diffracted to a high resolution and data were collected and processed at 1.63 Å (Table 1).

The overall structure (Figure 1) consists of two β-sheets and a short α-helix at the C-terminal end, identical with the crystal structure of PKCδC1B (PDB code 1PTQ) [22]. The two β-sheets formed a V-shaped activator-binding groove. Two Zn^{2+} ions were detected in the structure, each of which co-ordinates with three cysteine residues and a histidine residue. One Zn^{2+} co-ordinates with Cys^{261}, Cys^{264}, Cys^{280} and His^{231}, whereas the other co-ordinates with Cys^{247}, Cys^{244}, Cys^{272} and His^{269}. A total number of 129 water molecules were present in the structure. PKCθC1B has a high sequence homology (80%) and structural similarity with the crystal structure of PKCδC1B (PDB code 1PTQ) with an rmsd (root mean square deviation) of 0.66. However, the activator-binding pocket opening of PKCθC1B is slightly narrower (7.56 Å) than that of PKCδC1B (8.08 Å) owing to the upward orientation of the Trp^{253} at the rim of the activator-binding pocket opening. Superimposition of the crystal structure of PKCδC1B (PDB code 1PTR), complexed with phorbol 13-*O*-acetate (blue), with that of the PKCθC1B (pink) showed that all the homologous residues were superimposable except for the Trp^{253} residue (Figure 2). In PKCθC1B the Trp^{253} was orientated towards the membrane-binding region of the C1B subdomain, whereas the corresponding homologous Trp^{252} in PKCδC1B was orientated away from the membrane-binding region of the C1B subdomain (Figure 8A). Binding of the activator to the CI domain caps the hydrophilic activator-binding cavity and makes the membrane-binding surface more hydrophobic, aiding in the membrane anchoring. The upward orientation of Trp^{253} in PKCθC1B was not due to the crystal packing effect and this

has been further confirmed by the recently described NMR structure of PKCθC1B (PDB code 2ENZ) in which the Trp^{253} was also orientated upwards. While comparing our PKCθC1B crystal structure (PDB code 4FKD) with the NMR structure, it was found that the activator-binding pocket opening and the depth of pocket in the NMR structure (8.72 Å and 20.75 Å respectively) are slightly bigger than in the crystal structure (7.56 Å and 19.49 Å respectively).

The crystal structure also revealed that the nine extra residues (GSRRASVGS) at the N-terminus and the six extra residues (EFIVTD) in the C-terminus, which were added during subcloning of the corresponding gene in the pGEX2TK vector, formed two parallel β-sheets. These extra residues presumably stabilized the overall PKCθC1B structure for crystal formation. A similar observation was made recently with the PKCδC1B crystals [46].

Although an activator-bound structure of PKCθC1B would be able to identify the protein residues directly involved in activator binding, attempts with several hundred precipitants and conditions did not yield any protein–ligand co-crystals. Furthermore, soaking experiments with different activator solutions were also unsuccessful owing to the solubility problems of the activators in aqueous buffer. This highlights the importance of developing new molecules that would show improved aqueous solubility, yet would possess high binding affinity. Therefore we performed molecular docking of a library of DAG and phorbol esters using PKCθC1B as the receptor and sequence alignment of PKCθC1B and PKCδC1B to identify the possible activator-binding residues (Figure 2).

Molecular docking

In the phorbol 13-*O*-acetate-bound PKCδC1B structure (PDB code 1PTQ) [22], Gly^{253}, Thr^{242} and Leu^{251} form two, two and one hydrogen bonds respectively with phorbol 13-*O*-acetate. A sequence alignment of PKCθC1B with PKCδC1B showed that PKCθC1B consists of the same set of residues at the homologous position to the activator-binding residues in PKCδC1B, indicating similar binding could be possible with phorbol 13-*O*-acetate (Figure 2) [22]. Additionally, in the activator-binding region of PKCθC1B, there were other residues (Tyr^{239}, Thr^{243}, Trp^{253}, Leu^{255} and Gln^{258}) homologous to PKCδ, which could also play a role in activator binding. Our docking results revealed that the residues we identified from sequence alignment were also capable of forming hydrogen bonds with the docked activators.

Phorbol ester and DAG binding of PKCθC1B and its mutants

To determine the role of the above-mentioned residues in activator binding, Y239A, T243A, W253G, L255G and Q258G mutants were generated and their binding affinities for PDBu (K_d), DOG (K_i) and SAG (K_i) were measured. To study the role of the side chains responsible for ligand binding, the corresponding residues are usually mutated to alanine. However, mutation with glycine is not uncommon in the PKC activator-binding studies [21,28,29,47–51] and in the case of the δC1 domain, the mutational effect caused by either alanine or glycine has been found to be comparable [47]. To compare with the published data for the PKCδ mutants, we made several glycine mutants.

The K_d values for PDBu binding were in the nanomolar range and the mutants showed reduced affinity compared with the wild-type PKCθC1B (Table 2). Representative plots of PDBu binding to wild-type PKCθC1B and mutant L255G are shown in Figure 3. The K_d values of PDBu binding to Y239A, T243A, W253G, L255G and Q258G showed reductions of 8.51-, 1.64-, 7.56-, 11.4- and 1720-fold respectively compared with the wild-type (Figure 3 and Table 2). These data indicated that Q258G had a pronounced effect, whereas T243A has the least effect on PDBu binding. When binding affinities (K_i) of DOG were measured, Y239A, T243A, W253G, L255G and Q258G showed 5.34-, 1.34-, 29.2-, 4.72- and 114-fold reductions respectively, compared with the wild-type (Figure 3 and Table 2). In this case, Q258G showed the highest reduction in binding affinities and T243A showed the lowest effect. Finally, SAG showed a basically similar pattern as did DOG. Compared with the wild-type, Y239A, T243A, W253G, L255G and Q258G showed 4.13-, 0.63-, 31.1-, 8.16- and 260-fold reductions in binding affinities respectively. These data indicated that glutamine was the most critical among all mutated residues tested in the present study. For both DOG and SAG, W253G showed the second greatest effect, but this was not evident for PDBu. The relatively greater importance of a tryptophan residue at this position in other PKC isoforms for DAG binding, as compared with phorbol ester binding, has been described previously [52]. The C1B domain of PKCθ was reported to bind better to vesicles containing SAG than to those containing 1,2-dioleoylglycerol [53]. Consistent with that observation, we observed a 2-fold stronger binding affinity for SAG than for DOG.

To determine the effect of composition of anionic PS on activator binding, we determined radioactive PDBu binding by PKCθC1B and its mutants in the presence of varying proportions of PS in PS/PC mixtures while maintaining a fixed concentration of total phospholipid.

Effect of the phospholipid composition on [^{3}H]PDBu binding

Binding of [^{3}H]PDBu to PKCθC1B showed a marked dependence on the presence of PS, with essentially no binding observed in the presence of 100% PC (Figure 4). Approximately 30% binding was observed at 5% PS and maximal binding was attained with PS percentages between 75% and 100%. The T243A mutant showed almost the same dependence on PS as did the wild-type. On the other hand, mutants W253G and L255G showed appreciably greater dependence on PS for binding than did the wild-type, with 25% PS required, yielding the same level of binding observed in the wild-type at 5% PS. Finally, for both L255G and Y239A, maximal binding was obtained at 50–75% PS, with a decrease at 100%, whereas for the wild-type binding was maximal and constant between 75 and 100% PS.

As analysed by surface plasmon resonance [21], the W253G and L255G mutants of PKCθ showed significant reduction in the binding affinity (6- and 14-fold respectively) for DiC_{18} in lipid vesicles [POPC (1-palmitoyl-2-oleoyl phosphatidylcholine)/POPS(1-palmitoyl-2-oleoyl phosphatidylserine)/DiC_{18} = 69:30:1, by vol.]. This reduction is more than that of the corresponding homologous residues W181G and L183G (1.7- and 1.6-fold respectively) in C1A. Taken together, our data clearly indicate that the concentration of PS strongly affects the activator-binding affinity and the extent of this variation is different for different mutants.

The effect of PS on the activator binding for the homologous sites of PKCδ revealed that Leu^{250} and Leu^{255} of PKCδC1B strongly influenced the binding of PDBu [54]. The L250D and L255D mutations completely abolished the strong binding of PDBu in the presence or absence of PS. Also, the L250R and L255K mutations caused dramatic 340- and 250-fold reductions respectively in PDBu binding in the presence of lipid. Only a modest reduction in the PDBu binding (6.6- and 2.9-fold respectively) was observed in the absence of lipid. Mutation of L250K or W252K had a 3-fold effect compared with the wild-type in the presence of PS, whereas their binding affinity remained almost the same in the absence of the PS. At 50% PS, where PKCδC1B showed activity of approximately 100%, its W252K mutant showed approximately 55% of the maximum activity [54]. In the present study we found that, at 50% PS, PKCθC1B and its mutants Y239A, T243A, W253G, L255G and Q258G showed 90.5%, 130.7%, 98.2%, 59.3%, 92.8% and 85.7% of the level of PDBu binding observed at 100% PS respectively (Figure 4). The highest reduction observed for the W253A indicated that the Trp^{253} was critical for its interaction with membranes and subsequently the PDBu binding.

It is important to note that the present study using PKCθC1B was performed with GST-cleaved C1B constructs, whereas those reported for PKCδC1B were done with proteins in which the GST had not been cleaved. In any case, our results emphasize for PKCθC1B, as for other C1 domains, that measured binding represents the ternary complex of ligand, C1 domain and phospholipid, with all three elements contributing to the energetics of binding. Differences in the composition of various cellular phospholipids may thus make important contributions to ligand selectivity.

After measuring the binding affinities of phorbol ester and DAG to PKCθC1B and its mutants and the dependence on PS of their binding, we determined the effect of the mutations on the membrane translocation of the full-length kinase.

Effect of mutation in the C1B domain on membrane translocation

Translocation was measured separately in the presence of 50 nM PMA and 250 nM DOG. Activator-induced membrane translocation was quantified by the decrease of PKCθ and its mutants in the cytoplasmic pool (or the increase of the membrane pool). In the presence of 50 nM PMA, translocation was observed both for the wild-type PKCθ and for all mutants. Y239A, T243A, W253G, L255G and Q258G showed 17.1%, 12.5%, 14.8%, 19.4% and 21.6% reductions respectively in membrane translocation compared with the wild-type (Figure 5A). In the presence of 250 nM DOG, Y239A, T243A, W253G, L255G and Q258G showed 12.0%, 8.98%, 5.9%, 15.4% and 15.9% reduction in membrane translocation respectively compared with the wild-type (Figure 5B).

These results indicated that the residues mutated were important for the membrane translocation of the full-length kinase. Among the residues, Gln^{258} was found to be the most important, because mutation of Gln^{258} showed significant reduction in membrane translocation in the presence of both PMA and DOG. However, the mutational effect depended on the activator type, as evident in the comparison of PMA with DOG in full-length mutant translocation. The percentage reduction of the mutant translocation was somewhat greater in the presence of PMA compared with DOG.

Translocation of GFP–PKCθ wild-type and mutants in living LNCaP cells in response to PMA

Using the GFP-tagged PKCθ wild-type and mutants, we examined the sensitivity, kinetics and cellular localization of translocation in living cells in response to PMA. The constructs were expressed in LNCaP human prostate cancer cells because this cell line spreads well on the substratum, permitting good visualization, and has been extensively used for the analysis of PKC translocation. Representative images are shown in Figure 6. The images from all of the experiments were then quantified in terms of the signal/intensity ratio for membrane/cytoplasm (Table 3). At 10 nM PMA, negligible response was observed for all of the constructs (Table 3). At 100 nM PMA, the GFP–PKCθ wild-type showed marked translocation to the plasma membrane within 2 min (Figure 6). For T243A, translocation had begun within 2 min and was largely complete by 5 min. By 20 min, plasma membrane translocation was largely complete for all constructs, except Q258G, which showed little response. At 1000 nM PMA, the same pattern was evident, but with more extensive and faster translocation, and partial translocation of Q258G could now be seen at the later times. Although the constructs differed in their sensitivity and kinetics of response to PMA-induced translocation, in all cases translocation was to the plasma membrane.

DISCUSSION

PKCθ is unique among all the PKCs, because of its predominant expression in T-cells. It is the only PKC isoform which is uniquely targeted to the immunological synapse in T-cells and involved in the T-cell activation process [55,56]. We undertook this study to identify the activator-binding residues of the PKCθC1B subdomain and to accurately define the shape of the binding cleft with the future goal of designing PKCθ-specific molecules. A previous study by Melowic et al. [21] demonstrated a dominant role of the C1B subdomain in the membrane binding and activation process of PKCθ over CIA, its other (twin) cysteine-rich subdomain.

To identify the activator-binding residues, we first determined the crystal structure of the C1B domain at 1.63 Å resolution and used this structure to dock several known phorbol ester and DAG analogues to identify the possible residues in the protein that interact with these activators. Furthermore, by comparison with the activator-binding residues of PKCδC1B, for which the activator-bound structure is known [22], we identified five possible residues that could affect the activator binding.

Since the binding of DAG and phorbol ester to PKC showed differences in its dependence on structural features of the C1 domains [22,29,57–59], we used both phorbol ester and DAG for the present study. Our results indicated that, for PKCθC1B and its mutants, phorbol ester had higher binding affinity than DAG. Although to different extents, all the mutants showed reduced binding affinities for both phorbol ester and DAG as compared with the wild-type PKCθC1B. Out of the five residues that were tested, Gln^{258}, a conserved residue among the PKC isoforms, showed maximum influence both for binding by the phorbol ester and DAG and for membrane translocation in response to these ligands.

A careful inspection of the PKCθC1B structure revealed that Gln^{258} stabilizes the activator-binding pocket by bridging the left and the right activator-binding clefts. The backbone amine nitrogen of Gln^{258} could form a hydrogen bond (3.61 Å) with the backbone carbonyl oxygen of Tyr^{239} and the side-chain nitrogen (NE2) of Gln^{258} could form another hydrogen bond (2.87 Å) with the backbone carbonyl oxygen of Gly^{253}. Mutation of Gln^{258} with glycine resulted in the disruption of this bridge, leading to the highest reduction of binding affinity and membrane translocation.

Interestingly, under our binding conditions, W253G caused only a 4-fold greater loss of affinity for DOG than it did for PDBu. In the case of the C1B domain of PKCβI/II and PKCα under different lipid conditions, the presence of a tryptophan residue in place of tyrosine (Figure 7) greatly influenced binding of DAG, but not that of phorbol ester [52,60].

A comparison of the crystal structures of PKCδC1B and PKCθC1B revealed remarkable similarity of the overall structure. PKCθC1B has a high sequence homology (80%) with PKCδC1B (PDB code 1PTQ) with an rmsd of 0.66, indicating the similarity between the structures. Superimposition of the PKCθC1B structure with the PKCδC1B showed that the activator-binding pocket opening of PKCθC1B is slightly narrower than is that of the PKCδC1B. Another prominent difference is that, in the activator-binding surface, Met^{239} in PKCδC1B is replaced by Lys^{240} in PKCθC1B (Supplementary Figure S3 at http://www.biochemj.org/bj/451/bj4510033add.htm). This suggests that the affinity for the PS-rich membrane would be different for PKCθC1B and PKCδC1B.

Although the orientations for most of the residues of both the structures are almost identical, the orientation of Trp^{253} is totally opposite in these two structures (Figure 8). In a representation of the structure where the activator-binding loops are positioned towards the membrane, Trp^{253} is found to be orientated towards the membrane in PKCθC1B, whereas the homologous Trp^{252} of PKCδC1B is orientated downwards away from the membrane. Because of this particular orientation of Trp^{253} in PKCθC1B, its interactions with nearby residues are distinctly different from PKCδC1B. In PKCδC1B the indole ring of homologous Trp^{252} is found to be orientated in parallel to the imidazole ring of His^{270} at a distance of 4.13 Å, possibly involved in jr-stacking interactions [61–63]. In the PKCθC1B, however, similar interactions between the Trp^{253} and His^{270} are absent because these two rings are far apart (>10 Å) from each other (Figure 8). The pK_a of the imidazole ring nitrogen being ~6.0 means it would exist mostly in its neutral form at the physiological pH. Furthermore, since this histidine residue co-ordinates with one of the Zn^{2+} atoms, its possibility of existing as a cation is completely ruled out. The ε-NH_2 of Lys^{271} in PKCδ, which is protonated at physiological pH and located at a distance of 5.12 Å from the imidazole ring of His^{267} and at a distance of 5.49 Å from the indole ring of Trp^{252}, is most likely to be involved in cation-*it* interactions with both the rings, for this type of interaction occurs within a distance of 6 Å [63–65]. In PKCθC1B, however, this lysine residue is replaced by Arg^{272}, which is involved in cation-π interactions with His^{270} at a distance of 3.81 Å. Furthermore, upward orientation of Trp^{253} at the rim of the activator-binding pocket of PKCθC1B may also exert additional hydrophobic interactions, with the activator facilitating its binding to the membrane.

Although the Trp^{253} side chain is not directly orientated inside the activator-binding loop like the homologous Trp^{588} in Munc13.1, which occludes the DAG-binding site [66], our binding data for W253G showed 8-, 29- and 31-fold reductions in the binding of PDBu, DOG and SAG respectively by the mutant as compared with the wild-type. Although binding data of the DiC_{18} and the purified full-length W253G showed a 6-fold reduction in binding affinity in SPR analysis in a previous study [21], the results from the present study also showed reduced membrane translocation for both PDBu and DiC_8. It is important to emphasize, in any case, that the crystallographic analysis was for the isolated C1B domain, whereas ligand binding is measured in the presence of phospholipid. The orientations of Trp^{253} will undoubtedly be influenced by the presence of lipid and the effect of the W253G mutation will reflect, among other factors, its impact on the C1B-membrane interaction. Furthermore, comparison with other known C1 domain structures reveals that β2-chimerin [67] also has the homologous tryptophan residue in an orientation opposite to that of PKCθC1B.

Our binding data revealed that there were differences in the binding affinities of the mutants of PKCδ and PKCθ, particularly for W253G and L255G. In PKCθC1B, W253G and L255G showed 8- and 11-fold reductions respectively in their affinities for PDBu as compared with the wild-type. On the other hand, in PKCδC1B, the homologous mutants W252G and L254G showed 31- and > 1000-fold reductions, respectively. For Gln^{258} and Thr^{243}, mutation caused similar reductions of PDBu affinity for both PKCδ and PKCθ. For the Tyr^{239} site, the Y239A in PKCθC1B showed a 9-fold reduction; the homologous Y238G in PKCδC1B showed a 60-fold reduction in the binding affinity (Supplementary Table S1 at http://www.biochemj.org/bj/451/bj4510033add.htm). This is not surprising, since each mutation can cause a change in overall lipophilicity of the domain. Correspondingly, we found that the mutants differed in their PS dependence for phorbol ester binding. Whether the difference at the Tyr^{239} site between PKCθC1B and PKCδC1B is because of the different substitutions, alanine versus glycine respectively, or is a true reflection of the difference between PKCδ and θ is a matter of further investigation. Our modelling and molecular dynamics studies on Y238A and Y238G, however, showed that there was no significant structural change between the two mutants and both of them form four hydrogen bonds with PDBu. That the same residues in the two different isoforms with similar structures showed differential ligand-binding affinities indicated that there were cumulative effects, including the other nearby residues in determining the binding affinity, along with possible differences in their influence on membrane binding.

What are the key determinants for a C1 domain to be phorbol ester/DAG-responsive? The current concept is that PKC C1 domains anchor to the membranes as a ternary system including C1 domains, C1 activators and the anionic phospholipids present in the membrane, which bind to the positively charged residues present above the rim of the activator-binding cleft [28,29,68–70]. Alteration of any component in this ternary system, therefore, is expected to affect the ligand-binding affinity. For example, in the atypical PKCζ, several arginine residues lining the activator-binding pocket are responsible for its unresponsiveness towards the activator [71]. It has been suggested that these arginine residues reduce access of ligands to the binding cleft and change the electrostatic profile of the C1 domain surface, without altering the basic structure of the binding cleft. In Vav1C1, the presence of Glu^{9},

Glu[10], Thr[11], Thr[24] and Tyr[26] along the rim of the binding cleft reduced the overall lipophilicity of the rim, impairing the membrane association and thereby preventing the formation of the ternary complex [45]. In Munc13.1, occlusion of Trp[588] in the activator-binding pocket reduces its affinity for the activators [66]. Our results of the present study emphasize that the structure and orientation of the residues are also important in determining the responsiveness of a C1 domain towards its activator.

In conclusion, our 1.63 Å structure of PKCθC1B revealed close similarity between the PKCδ and PKCθ C1B structures, except for the orientation of the Trp[253] residue, which plays a critical role in membrane binding. Out of the five residues, Gln[258] showed the most prominent effect on both activator binding and PKC translocation, with each site having its own contribution to the activator-binding affinity of the C1B subdomain.

Although the present study has identified several unique structural features in the activator-binding domain of PKCθC1B, further studies will be required to understand the mechanism by which PKCθ is specifically targeted to the immunological synapse of the T-cells.

Supplementary Material

Refer to Web version on PubMed Central for supplementary material.

ACKNOWLEDGEMENTS

We thank Dr Amnon Altman (La Jolla Institute for Allergy and Immunology, La Jolla, CA, U.S.A.) for providing the PKCθ construct. Molecular docking and dynamics were performed at the Center for Experimental Therapeutics and PharmacoInformatics (College of Pharmacy, University of Houston, Houston, TX, U.S.A.).

FUNDING

This research was supported in part by Startup funds from the University of Houston (to J.D.) and by the Intramural Program of the National Institutes of Health, Center for Cancer Research, National Cancer Institute [project number Z1A BC 005270].

Abbreviations used:

AP-1	activator protein 1
APC	antigen-presenting cell
DAG	diacylglycerol
DOG	*sn*-1,2-dioctanoylglycerol
DMEM	Dulbecco's modified Eagle's medium
EGFP	enhanced green fluorescent protein
FBS	fetal bovine serum
GFP	green fluorescent protein
GST	glutathione transferase

HEK	human embryonic kidney
HRP	horseradish peroxidase
MALDI–TOF-MS	matrix-assisted laser-desorption ionization–time-of-flight MS
NF-κB	nuclear factor κB
PC	L-α-phosphatidylcholine
PDBu	phorbol 12,13-dibutyrate
PKC	protein kinase C
PS	L-α-phosphatidylserine
rmsd	root mean square deviation
SAG	*sn*-1-stearoyl 2-arachidonyl glycerol
TB	terrific broth
TCR	T-cell receptor

REFERENCES

1. Mellor H and Parker PJ (1998) The extended protein kinase C superfamily. Biochem. J 332, 281–292 [PubMed: 9601053]
2. Baier G, Telford D, Giampa L, Coggeshall KM, Baier-Bitterlich G, Isakov N and Altman A (1993) Molecular cloning and characterization of PKCθ, a novel member of the protein kinase C (PKC) gene family expressed predominantly in hematopoietic cells. J. Biol. Chem 268, 4997–5004 [PubMed: 8444877]
3. Arendt CW, Albrecht B, Soos TJ and Littman DR (2002) Protein kinase C-θ: signaling from the center of the T-cell synapse. Curr. Opin. Immunol 14, 323–330 [PubMed: 11973130]
4. Isakov N and Altman A (2002) Protein kinase Cθ in T cell activation. Annu. Rev. Immunol 20, 761–794 [PubMed: 11861617]
5. Healy AM, Izmailova E, Fitzgerald M, Walker R, Hattersley M, Silva M, Siebert E, Terkelsen J, Picarella D, Pickard MD et al. (2006) PKC-θ-deficient mice are protected from Th1-dependent antigen-induced arthritis. J. Immunol 177, 1886–1893 [PubMed: 16849501]
6. Salek-Ardakani S, So T, Halteman BS, Altman A and Croft M (2004) Differential regulation of Th2 and Th1 lung inflammatory responses by protein kinase C θ. J. Immunol 173, 6440–6447 [PubMed: 15528385]
7. Salek-Ardakani S, So T, Halteman BS, Altman A and Croft M (2005) Protein kinase Cθ controls Th1 cells in experimental autoimmune encephalomyelitis. J. Immunol 175, 7635–7641 [PubMed: 16301673]
8. Manning G, Whyte DB, Martinez R, Hunter T and Sudarsanam S (2002) The protein kinase complement of the human genome. Science 298, 1912–1934 [PubMed: 12471243]
9. Cooke DW and Plotnick L (2008) Type 1 diabetes mellitus in pediatrics. Pediatr. Rev 29, 374–384 [PubMed: 18977856]
10. Marsland BJ, Soos TJ, Spath G, Littman DR and Kopf M (2004) Protein kinase C θ is critical for the development of in vivo T helper (Th)2 cell but not Th1 cell responses. J. Exp. Med 200, 181–189 [PubMed: 15263025]

11. Giannoni F, Lyon AB, Wareing MD, Dias PB and Sarawar SR (2005) Protein kinase C θ is not essential for T-cell-mediated clearance of murine gammaherpesvirus 68. J. Virol 79, 6808–6813 [PubMed: 15890920]
12. Nishizuka Y (1992) Intracellular signaling by hydrolysis of phospholipids and activation of protein kinase C. Science 258, 607–614 [PubMed: 1411571]
13. Altman A, Isakov N and Baier G (2000) Protein kinase Cθ: a new essential superstar on the T-cell stage. Immunol. Today 21, 567–573 [PubMed: 11094261]
14. Nishizuka Y (1995) Protein kinase C and lipid signaling for sustained cellular responses. FASEB J. 9, 484–496 [PubMed: 7737456]
15. Irie K, Oie K, Nakahara A, Yanai Y, Ohigashi H, Wender PA, Fukuda H, Konishi H and Kikkawa U (1998) Molecular basis for protein kinase C isozyme-selective binding: the systhesis, folding, and phorbol ester binding of the cysteine-rich domains of all protein kinase C isozymes. J. Am. Chem. Soc 120, 9159–9167
16. Newton AC (2001) Protein kinase C: structural and spatial regulation by phosphorylation, cofactors, and macromolecular interactions. Chem. Rev 101, 2353–2364 [PubMed: 11749377]
17. Downward J, Graves JD, Warne PH, Rayter S and Cantrell DA (1990) Stimulation of p21ras upon T-cell activation. Nature 346, 719–723 [PubMed: 2201921]
18. Chaudhary D and Kasaian M (2006) PKCθ: a potential therapeutic target for T-cell-mediated diseases. Curr. Opin. Investig. Drugs 7, 432–437
19. Blumberg PM, Kedei N, Lewin NE, Yang D, Czifra G, Pu Y, Peach ML and Marquez VE (2008) Wealth of opportunity – the C1 domain as a target for drug development. Curr. Drug Targets 9, 641–652 [PubMed: 18691011]
20. Irie K, Nakahara A, Nakagawa Y, Ohigashi H, Shindo M, Fukuda H, Konishi H, Kikkawa U, Kashiwagi K and Saito N (2002) Establishment of a binding assay for protein kinase C isozymes using synthetic C1 peptides and development of new medicinal leads with protein kinase C isozyme and C1 domain selectivity. Pharmacol. Ther 93, 271–281 [PubMed: 12191619]
21. Melowic HR, Stahelin RV, Blatner NR, Tian W, Hayashi K, Altman A and Cho W (2007) Mechanism of diacylglycerol-induced membrane targeting and activation of protein kinase Cθ. J. Biol. Chem 282, 21467–21476 [PubMed: 17548359]
22. Zhang G, Kazanietz MG, Blumberg PM and Hurley JH (1995) Crystal structure of the cys2 activator-binding domain of protein kinase Cδ complex with phorbol ester. Cell 81, 917–924 [PubMed: 7781068]
23. Kaelin Jr W. G., Krek W, Sellers WR, DeCaprio JA, Ajchenbaum F, Fuchs CS, Chittenden T, Li Y, Farnham PJ, Blanar MA. et al. (1992) Expression cloning of a cDNA encoding a retinoblastoma-binding protein with E2F-like properties. Cell 70, 351–364 [PubMed: 1638635]
24. Charoenthongtrakul S, Zhou Q, Shembade N, Harhaj NS and Harhaj EW (2011) Human T cell leukemia virus type 1 Tax inhibits innate antiviral signaling via NF-κB-dependent induction of SOCS1. J. Virol 85, 6955–6962 [PubMed: 21593151]
25. Kunkel TA (1985) Rapid and efficient site-specific mutagenesis without phenotypic selection. Proc. Natl. Acad. Sci. U.S.A 82, 488–492 [PubMed: 3881765]
26. Sugimoto M, Esaki N, Tanaka H and Soda K (1989) A simple and efficient method for the oligonucleotide-directed mutagenesis using plasmid DNA template and phosphorothioate-modified nucleotide. Anal. Biochem 179, 309–311 [PubMed: 2549807]
27. Nelson M and McClelland M (1992) Use of DNA methyltransferase/endonuclease enzyme combinations for megabase mapping of chromosomes. Methods Enzymol 216, 279–303 [PubMed: 1336094]
28. Stahelin RV, Digman MA, Medkova M, Ananthanarayanan B, Rafter JD, Melowic HR and Cho W (2004) Mechanism of diacylglycerol-induced membrane targeting and activation of protein kinase Cδ. J. Biol. Chem 279, 29501–29512 [PubMed: 15105418]
29. Stahelin RV, Digman MA, Medkova M, Ananthanarayanan B, Melowic HR, Rafter JD and Cho W (2005) Diacylglycerol-induced membrane targeting and activation of protein kinase Cε: mechanistic differences between protein kinases Cδ and Cε. J. Biol. Chem 280, 19784–19793 [PubMed: 15769752]

30. Quest AF, Bardes ES, Xie WQ, Willott E, Borchardt RA and Bell RM (1995) Expression of protein kinase Cγ regulatory domain elements containing cysteine-rich zinc-coordinating regions as glutathione S-transferase fusion proteins. Methods Enzymol. 252, 153–167 [PubMed: 7476349]
31. Das J, Pany S, Rahman GM and Slater SJ (2009) PKCε has an alcohol-binding site in its second cysteine-rich regulatory domain. Biochem. J 421, 405–413 [PubMed: 19432558]
32. Leonard TA, Rozycki B, Saidi LF, Hummer G and Hurley JH (2011) Crystal structure and allosteric activation of protein kinase C βII. Cell 144, 55–66 [PubMed: 21215369]
33. Littler DR, Walker JR, She YM, Finerty PJ Jr, Newman EM and Dhe-Paganon S (2006) Structure of human protein kinase C η (PKCη) C2 domain and identification of phosphorylation sites. Biochem. Biophys. Res. Commun 349, 1182–1189 [PubMed: 16973127]
34. Collaborative Computational Project, Number 4 (1994) The CCP4 suite: programs for protein crystallography. Acta Crystallogr. Sect. D Biol. Crystallogr 50, 760–763 [PubMed: 15299374]
35. Evans P (2006) Scaling and assessment of data quality. Acta Crystallogr. Sect. D Biol. Crystallogr 62, 72–82 [PubMed: 16369096]
36. McCoy AJ, Grosse-Kunstleve RW, Adams PD, Winn MD, Storoni LC and Read RJ (2007) Phaser crystallographic software. J. Appl. Crystallogr 40, 658–674 [PubMed: 19461840]
37. Langer G, Cohen SX, Lamzin VS and Perrakis A (2008) Automated macromolecular model building for X-ray crystallography using ARP/wARP version 7. Nat. Protoc 3, 1171–1179 [PubMed: 18600222]
38. Winn MD, Murshudov GN and Papiz MZ (2003) Macromolecular TLS refinement in REFMAC at moderate resolutions. Methods Enzymol. 374, 300–321 [PubMed: 14696379]
39. Emsley P and Cowtan K (2004) Coot: model-building tools for molecular graphics. Acta Crystallogr. Sect. D Biol. Crystallogr 60, 2126–2132 [PubMed: 15572765]
40. Dundas J, Ouyang Z, Tseng J, Binkowski A, Turpaz Y and Liang J (2006) CASTp: computed atlas of surface topography of proteins with structural and topographical mapping of functionally annotated residues. Nucleic Acids Res. 34, W116–W118 [PubMed: 16844972]
41. Lewin NE and Blumberg PM (2003) [^{3}H]Phorbol 12,13-dibutyrate binding assay for protein kinase C and related proteins. Methods Mol. Biol 233, 129–156 [PubMed: 12840504]
42. Das J, Pany S and Majhi A (2011) Chemical modifications of resveratrol for improved protein kinase Cα activity. Bioorg. Med. Chem 19, 5321–5333 [PubMed: 21880495]
43. Chen N, Ma W, Huang C and Dong Z (1999) Translocation of protein kinase Cε and protein kinase Cδ to membrane is required for ultraviolet B-induced activation of mitogen-activated protein kinases and apoptosis. J. Biol. Chem 274, 15389–15394 [PubMed: 10336426]
44. Slater SJ, Kelly MB, Taddeo FJ, Rubin E and Stubbs CD (1994) Evidence for discrete diacylglycerol and phorbol ester activator sites on protein kinase C. Differences in effects of 1-alkanol inhibition, activation by phosphatidylethanolamine and calcium chelation. J. Biol. Chem 269, 17160–17165 [PubMed: 8006023]
45. Geczy T, Peach ML, El Kazzouli S, Sigano DM, Kang JH, Valle CJ, Selezneva J, Woo W, Kedei N, Lewin NE et al. (2012) Molecular basis for the failure of the “atypical” C1 domain of Vav1 to bind diacylglycerol/phorbol ester. J. Biol. Chem 287, 13137–13158 [PubMed: 22351766]
46. Shanmugasundararaj S, Das J, Sandberg WS, Zhou X, Wang D, Messing RO, Bruzik KS, Stehle T and Miller KW (2012) Structural and functional characterization of an anesthetic binding site in the second cysteine-rich domain of protein kinase Cδ. Biophys. J 103, 2331–2340 [PubMed: 23283232]
47. Kazanietz MG, Wang S, Milne GW, Lewin NE, Liu HL and Blumberg PM (1995) Residues in the second cysteine-rich region of protein kinase Cδ relevant to phorbol ester binding as revealed by site-directed mutagenesis. J. Biol. Chem 270, 21852–21859 [PubMed: 7665608]
48. Schultz A, Ling M and Larsson C (2004) Identification of an amino acid residue in the protein kinase C C1b domain crucial for its localization to the Golgi network. J. Biol. Chem 279, 31750–31760 [PubMed: 15145947]
49. Kashiwagi K, Shirai Y, Kuriyama M, Sakai N and Saito N (2002) Importance of C1B domain for lipid messenger-induced targeting of protein kinase C. J. Biol. Chem 277, 18037–18045 [PubMed: 11877428]

50. Lopez-Nicolas R, Lopez-Andreo MJ, Marin-Vicente C, Gomez-Fernandez JC and Corbalan-Garcia S (2006) Molecular mechanisms of PKCα localization and activation by arachidonic acid. The C2 domain also plays a role. J. Mol. Biol 357, 1105–1120 [PubMed: 16476439]
51. Pak Y, Enyedy IJ, Varady J, Kung JW, Lorenzo PS, Blumberg PM and Wang S (2001) Structural basis of binding of high-affinity ligands to protein kinase C: prediction of the binding modes through a new molecular dynamics method and evaluation by site-directed mutagenesis. J. Med. Chem 44, 1690–1701 [PubMed: 11356104]
52. Dries DR, Gallegos LL and Newton AC (2007) A single residue in the C1 domain sensitizes novel protein kinase C isoforms to cellular diacylglycerol production. J. Biol. Chem 282, 826–830 [PubMed: 17071619]
53. Carrasco S and Merida I (2004) Diacylglycerol-dependent binding recruits PKCθ and RasGRP1 C1 domains to specific subcellular localizations in living T lymphocytes. Mol. Biol. Cell 15, 2932–2942 [PubMed: 15064353]
54. Wang QJ, Fang TW, Nacro K, Marquez VE, Wang S and Blumberg PM (2001) Role of hydrophobic residues in the C1b domain of protein kinase Cδ on ligand and phospholipid interactions. J. Biol. Chem 276, 19580–19587 [PubMed: 11278612]
55. Monks CR, Kupfer H, Tamir I, Barlow A and Kupfer A (1997) Selective modulation of protein kinase C-θ during T-cell activation. Nature 385, 83–86 [PubMed: 8985252]
56. Grakoui A, Bromley SK, Sumen C, Davis MM, Shaw AS, Allen PM and Dustin ML (1999) The immunological synapse: a molecular machine controlling T cell activation. Science 285, 221–227 [PubMed: 10398592]
57. Bazzi MD and Nelsestuen GL (1988) Properties of membrane-inserted protein kinase C. Biochemistry 27, 7589–7593 [PubMed: 3207690]
58. Kazanietz MG, Krausz KW and Blumberg PM (1992) Differential irreversible insertion of protein kinase C into phospholipid vesicles by phorbol esters and related activators. J. Biol. Chem 267, 20878–20886 [PubMed: 1400402]
59. Ananthanarayanan B, Stahelin RV, Digman MA and Cho W (2003) Activation mechanisms of conventional protein kinase C isoforms are determined by the ligand affinity and conformational flexibility of their C1 domains. J. Biol. Chem 278, 46886–46894 [PubMed: 12954613]
60. Stewart MD, Morgan B, Massi F and Igumenova TI (2011) Probing the determinants of diacylglycerol binding affinity in the C1B domain of protein kinase Cα. J. Mol. Biol 408, 949–970 [PubMed: 21419781]
61. McGaughey GB, Gagne M and Rappe AK (1998) π-Stacking interactions. Alive and well in proteins. J. Biol. Chem 273, 15458–15463 [PubMed: 9624131]
62. Wang L, Sun N, Terzyan S, Zhang X and Benson DR (2006) A histidine/tryptophan π-stacking interaction stabilizes the heme-independent folding core of microsomal apocytochrome b5 relative to that of mitochondrial apocytochrome b5. Biochemistry 45, 13750–13759 [PubMed: 17105194]
63. Dougherty DA (1996) Cation-π interactions in chemistry and biology: a new view of benzene, Phe, Tyr, and Trp. Science 271, 163–168 [PubMed: 8539615]
64. Gallivan JP and Dougherty DA (1999) Cation-π interactions in structural biology. Proc. Natl. Acad. Sci. U.S.A 96, 9459–9464 [PubMed: 10449714]
65. Takeuchi H, Okada A and Miura T (2003) Roles of the histidine and tryptophan side chains in the M2 proton channel from influenza A virus. FEBS Lett. 552, 35–38 [PubMed: 12972149]
66. Shen N, Guryev O and Rizo J (2005) Intramolecular occlusion of the diacylglycerol-binding site in the C1 domain of munc13–1. Biochemistry 44, 1089–1096 [PubMed: 15667202]
67. Canagarajah B, Leskow FC, Ho JY, Mischak H, Saidi LF, Kazanietz MG and Hurley JH (2004) Structural mechanism for lipid activation of the Rac-specific GAP, β2-chimaerin. Cell 119, 407–418 [PubMed: 15507211]
68. Giorgione JR, Lin JH, McCammon JA and Newton AC (2006) Increased membrane affinity of the C1 domain of protein kinase Cδ compensates for the lack of involvement of its C2 domain in membrane recruitment. J. Biol. Chem 281, 1660–1669 [PubMed: 16293612]
69. Slater SJ, Seiz JL, Cook AC, Buzas CJ, Malinowski SA, Kershner JL, Stagliano BA and Stubbs CD (2002) Regulation of PKCα activity by C1-C2 domain interactions. J. Biol. Chem 277, 15277–15285 [PubMed: 11850425]

70. Stahelin RV, Wang J, Blatner NR, Rafter JD, Murray D and Cho W (2005) The origin of C1A-C2 interdomain interactions in protein kinase Cα. J. Biol. Chem 280, 36452–36463 [PubMed: 16079140]

71. Pu Y, Peach ML, Garfield SH, Wincovitch S, Marquez VE and Blumberg PM (2006) Effects on ligand interaction and membrane translocation of the positively charged arginine residues situated along the C1 domain binding cleft in the atypical protein kinase C isoforms. J. Biol. Chem 281, 33773–33788 [PubMed: 16950780]

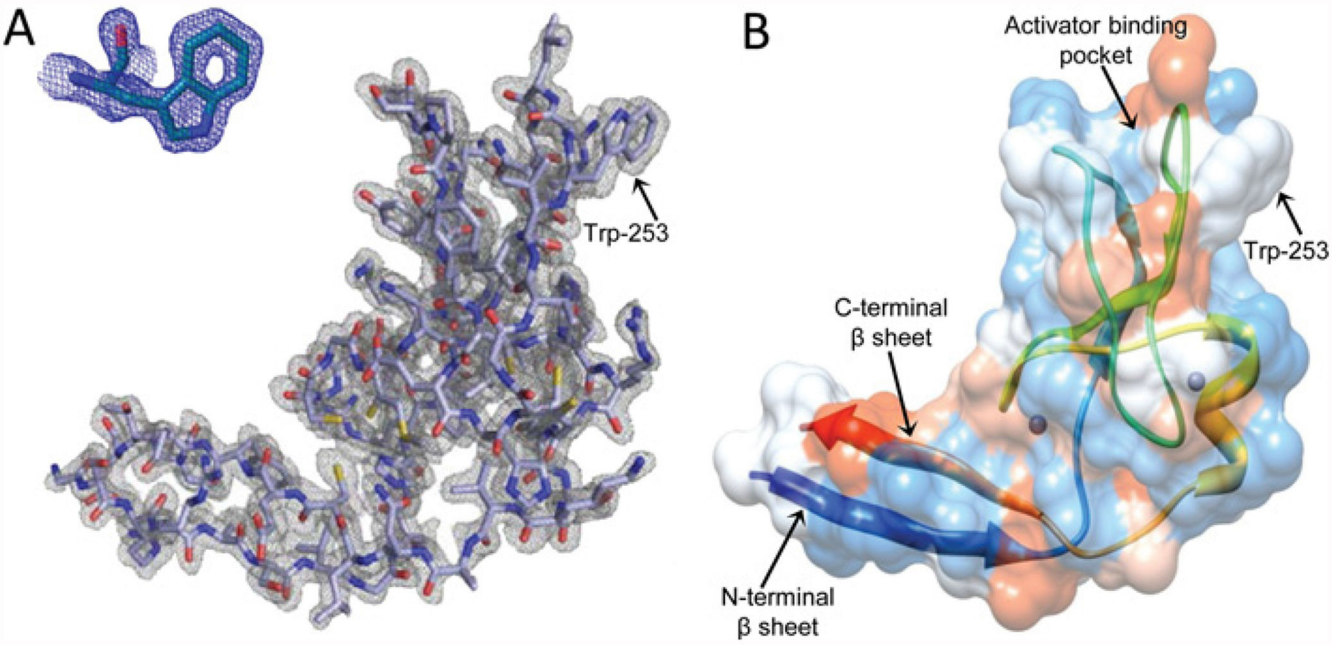

Figure 1. Structure of PKCθC1B

(**A**) Electron density map ($2F_0 - F_0$) of the PKCθC1B subdomain showing upward orientation of Trp^{253} towards the membrane. Expanded view of the electron density fit for Trp^{253} is shown in the top left-hand corner. (**B**) Ribbon structure of PKCθC1B superimposed on the contour surface. The blue area on the contour surface represents the polar residues, whereas the white to orange-red represents the most hydrophobic residues. Extra residues added to the N- and C-terminus form a β-sheet structure.

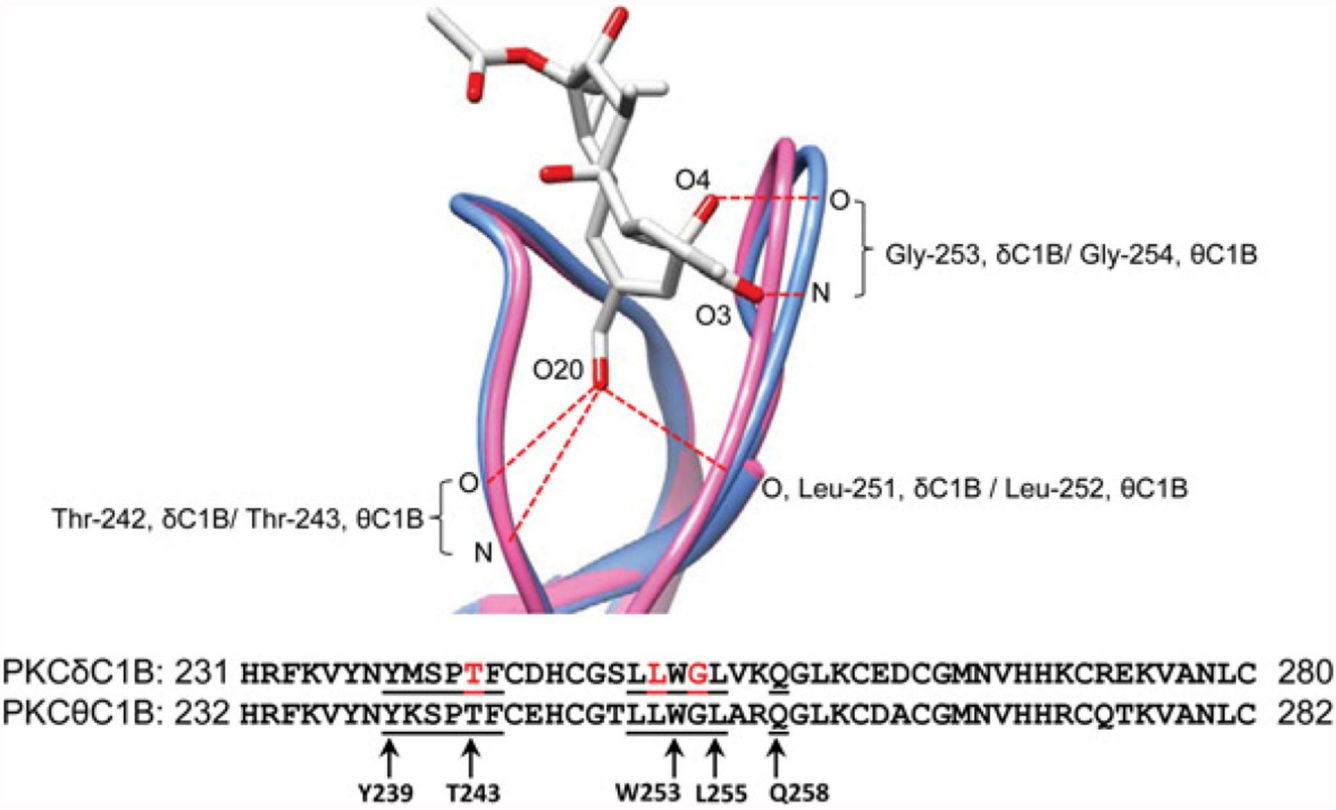

Figure 2. Structure and sequence comparison between PKC*δ*C1B and PKC*θ*C1B for identifying activator-binding residues

Overlay of the crystal structure of PKC*δ*C1B (blue) bound with phorbol-13-*O*-acetate and PKC*θ*C1B (pink) shows that they are superimposable. Phorbol-13-*O*-acetate forms five hydrogen bonds in the activator-binding groove of PKC*δ*C1B; two bonds with Gly^{253}, two bonds with Thr^{242}, and one bond with Leu^{251} (denoted with a dotted red line). PKC*θ*C1B consists of the same homologous activator-binding residues, indicating similar binding could be possible with phorbol-13-*O*-acetate upon co-crystallization. Residues underlined in the PKC*δ*C1B sequence constitute the activator-binding regions and the residues in red are the direct activator-binding residues reported in the co-crystallized structure (PDB code 1PTR). Residues marked with an arrow in PKC*θ*C1B are the residues that were mutated. Only the activator-binding portions of the C1B domains are shown in the Figure.

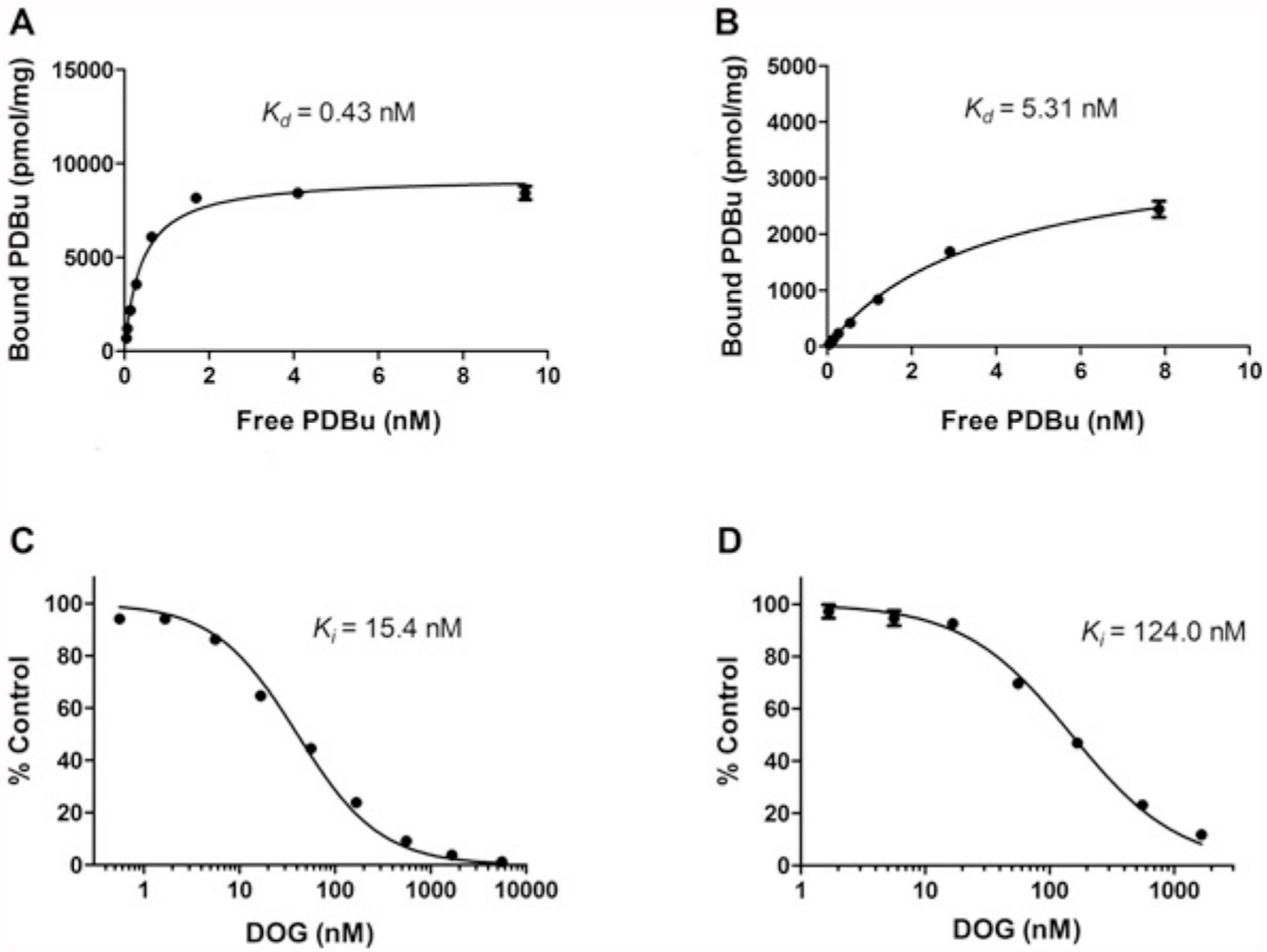

Figure 3. Determination of K_d and K_i

(**A** and **B**) Determination of K_d. Saturation plots for the binding of [^{3}H]PDBu to (**A**) PKCθC1B and (**B**) PKCθC1B L255G. (**C** and **D**) Determination of K_i. Plots for competitive inhibition of the binding of [^{3}H]PDBu by DOG to (**C**) PKCθC1B and (**D**) PKCθC1B L255G. The results are the means ° S.E.M. of the triplicate points in a single experiment. Where the error bars are not visible they are smaller than the symbol. The experiments illustrated are representative of triplicate experiments. The mean values for K_d and K_i are presented in Table 2.

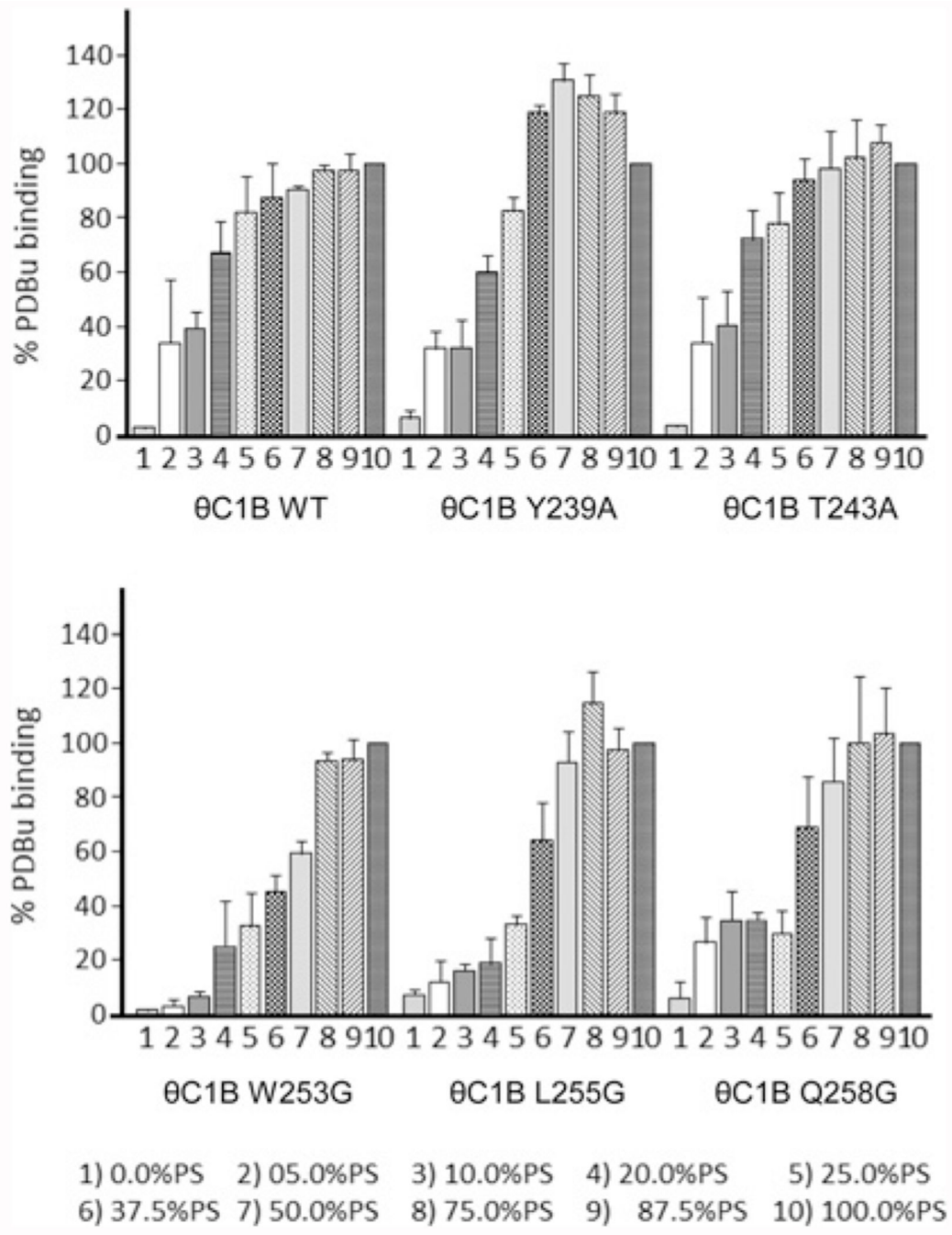

Figure 4. Effect of PS on phorbol ester binding

PDBu binding to PKC*θ*C1B and its mutants was determined as a function of the percentage of PS in PS/PC phospholipid mixtures and was expressed relative to binding at 100% PS. The results are the means ± S.E.M. of three independent experiments.

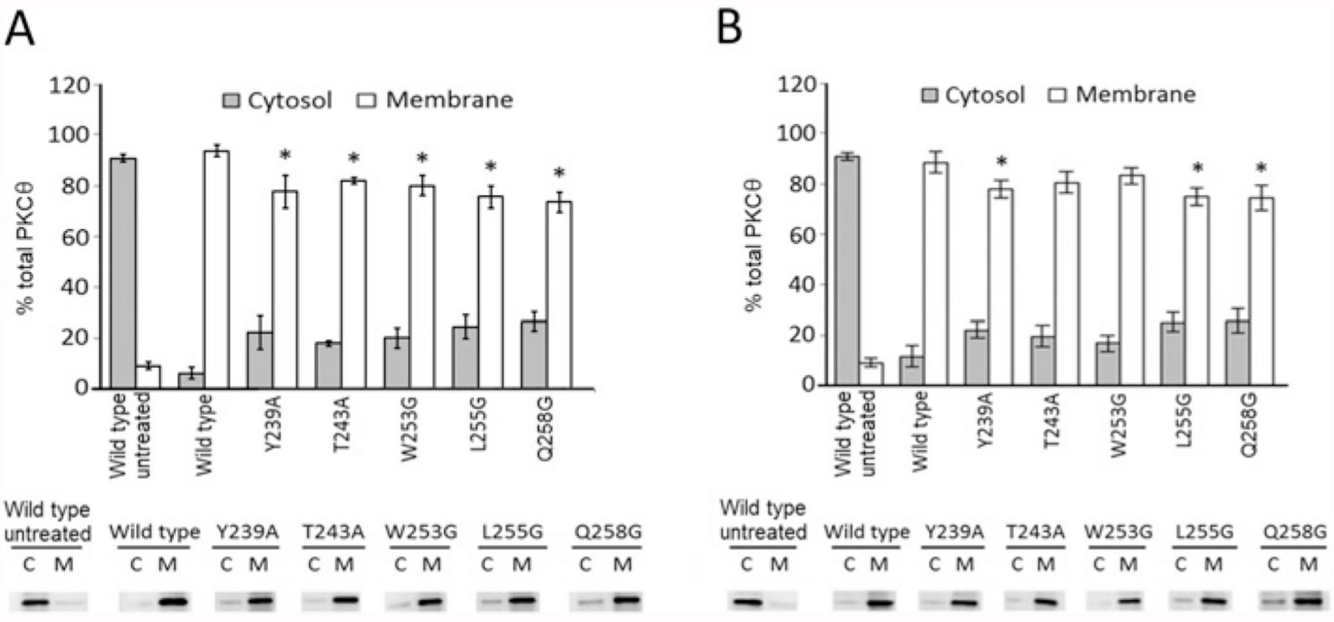

Figure 5. Effect of mutations on the membrane translocation properties of PKC*θ* and its C1B domain mutants

Distribution between cytosol and membrane of PKC*θ* and its mutants following treatment for 2 h with (**A**) 50 nM PMA, and (**B**) 250 nM DOG. Full-length proteins were expressed in HEK-293 cells. The cells were treated with either PMA or DOG, harvested and fractionated. The cytosolic (C) and membrane (M) fractions were analysed by Western blotting. Each data point represents the means ± S.D. of three measurements. **P* < 0.05.

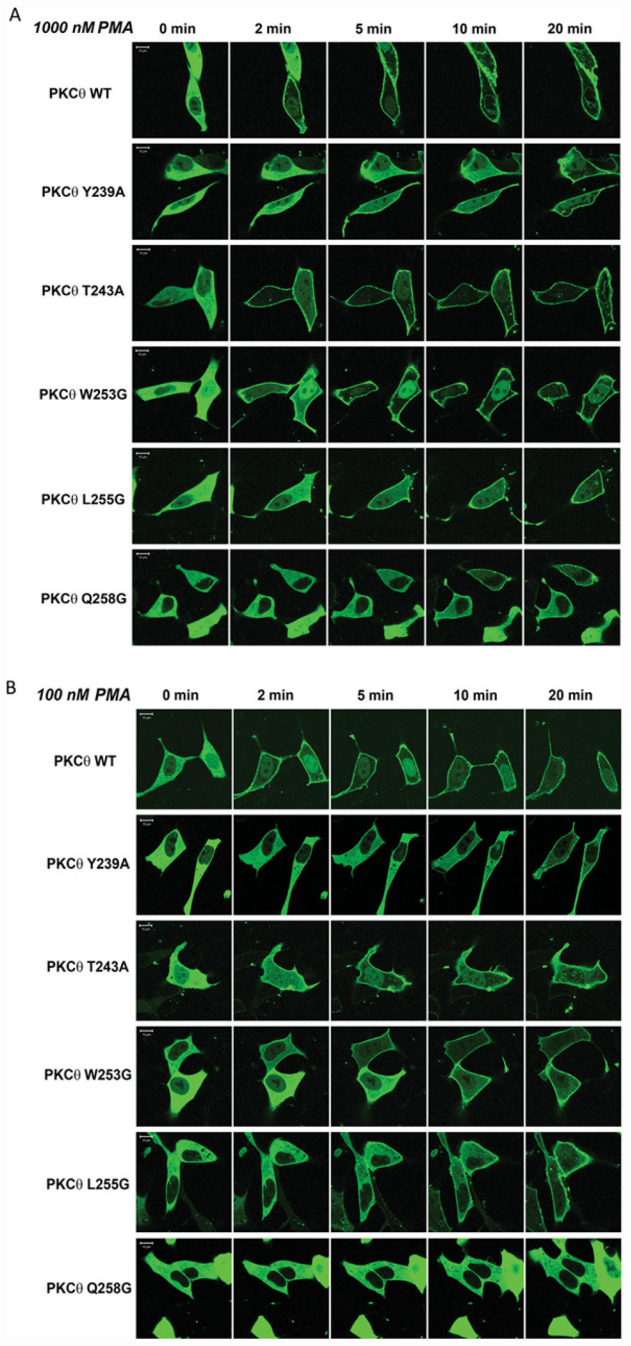

Figure 6. The translocation pattern of the GFP-tagged PKC*θ* wild-type and its mutants in living LNCaP cells after PMA treatment

Cells expressing the wild-type or mutant GFP–PKC*θ* constructs were treated with the 1000 nM (**A**) or 100 nM (**B**) PMA. The translocation pattern was examined by confocal microscopy as a function of time. Each panel represents images typical of three to four independent experiments.

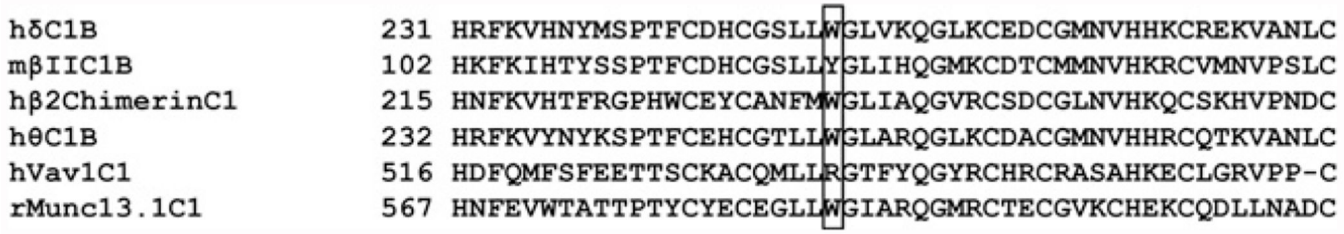

Figure 7. Sequence comparison of the C1 domains

The Trp^{253} in PKCθ and its homologous residues in other C1 domains are boxed.

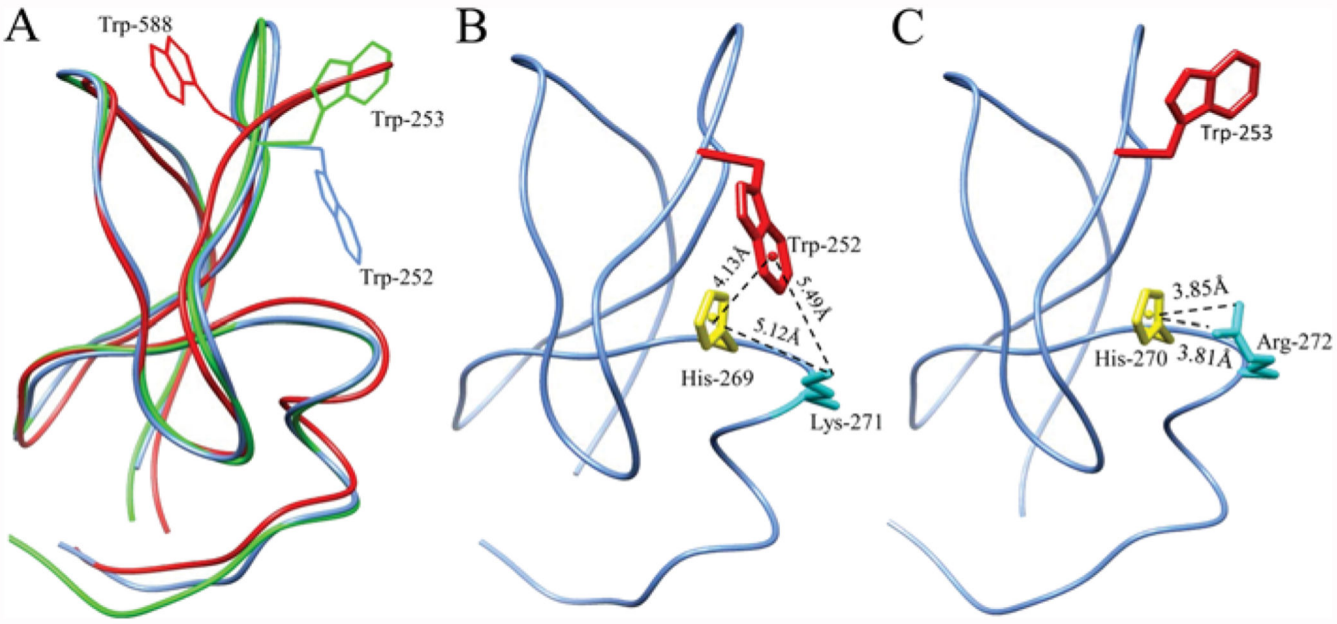

Figure 8. Orientation of the tryptophan residue in PKCδC1B, PKCθC1B and Munc 13.1 C1

(**A**) Orientation of Trp^{252} of PKCδC1B (blue), Trp^{253} of PKCθC1B (green) and Trp^{588} of Munc13.1C1 (red) at consensus position 22 in the overlaid structure of PKCδC1B (PDB code 1PTQ), PKCθC1B (PDB code 4FKD) and Munc 13-1 C1-domain (PDB code 1Y8F) respectively. Trp^{252} is orientated away from the membrane, whereas Trp^{253} is orientated towards the membrane. Trp^{588} of the Munc 13-1 C1 domain is projected inside the activator-binding pocket. (**B**) Possible π stacking interaction between Trp^{252} and His^{269} and cation–π interaction between Trp^{252} and Lys^{271} in PKCδC1B, and (**C**) possible cation–π interaction between His^{270} and Arg^{272} in PKCθC1B.

Table 1

PKCθC1B crystal data processing and refinement statistics

Values in brackets refer to the highest resolution shell. rms, root mean square.

Crystal parameters	Values
Space group	$P6_1$
Unit cell axis (Å)	$a = b = 65.85$, $c = 27.12$
Resolution (Å)	28.51–1.63 (1.72–1.63)
Total number of reflections	45483
Total number of unique reflections	7559
Redundancy	6.0
Completeness (%)	88.39 (98.00)
I/σ	18.6(9.7)
R_{merge}	0.044 (0.115)
R_{work}/R_{free} (%)	17.14/20.42
Wavelength	1.54178 Å (copper anode)
Distance (mm)	100
Number of water molecules	130
Wilson B-factor	15.2
B-factor	19.93
Number of metal atoms	2 Zn^{2+}
Bond length (Å, rms)	0.01
Bond angle (°, rms)	1.03

Table 2

Binding of PDBu and DOG to PKCθC1B domain variants

WT, wild-type.

	PKCθC1B WT	PKCθC1B Y239A	PKCθC1B T243A	PKCθC1B W253G	PKCθC1B L255G	PKCθC1B Q258G
PDBu K_d (nM) *	0.39 ± 0.2	3.32 ± 0.34	0.64 ± 0.06	2.95 ± 0.19	4.44 ± 0.56	670 ± 150
DOG K_i (nM) *	16.1 ± 0.7	86 ± 15	21.5 ± 1.8	470 ± 69	76 ± 24	1840 ± 320
K_i/K_d	41	26	34	159	17	3
SAG K_i (nM) *	8.7 ± 2.0	35.1 ± 5.1	5.5 ± 1.5	271 ± 22	71 ± 10	2260 ± 330
K_i/K_d	22	11	9	92	16	3

* Values represent the means ± S.E.M. of triplicate independent experiments.

Table 3

Quantification of membrane/cytoplasmic intensity ratios in confocal images

Membrane/cytoplasmic intensity ratios were calculated from the confocal images of the multiple experiments. Values are the means ± S.E.M. of at least three images for 1000 nM and 100 nM PMA-treated samples and at least two images for the 10 nM PMA treated samples. WT, wild-type.

Treatment	Time (min)	PKCθWT	PKCθY239A	PKCθT243A	PKCθW253G	PKCθL255G	PKCθQ258G
100 nM PMA	5	14.5 ± 2.2	3.8 ± 1.8	10.3 ± 1.9	11.4 ± 3.6	4.8 ± 1.5	1.2 ± 0.1
	10	11.3 ± 2.1	4.2 ± 1.6	9.9 ± 1.5	12.7 ± 3.9	6.0 ± 1.2	2.0 ± 0.3
	20	12.1 ± 2.2	5 ± 0.4	7.4 ± 1.5	13.2 ± 5.0	7.2 ± 1.9	2.1 ± 0.4
100 nM PMA	5	8.1 ± 1.2	1.7 ± 0.4	3.6 ± 1.1	1.9 ± 0.4	1.3 ± 0.1	1.0 ± 0.0
	10	6.5 ± 0.7	2.3 ± 0.8	3.7 ± 0.8	3.0 ± 0.7	1.6 ± 0.2	1.1 ± 0.0
	20	5.4 ± 0.5	2.3 ± 0.5	3.1 ± 0.6	2.6 ± 0.6	2.3 ± 0.4	1.1 ± 0.0
10 nM PMA	5	1.0 ± 0.1	1.1 ± 0.0	1.0 ± 0.0	1.0 ± 0.1	1.1 ± 0.1	1.2 ± 0.1
	10	1.0 ± 0.1	1.1 ± 0.1	1.3 ± 0.2	1.1 ± 0.1	1.1 ± 0.1	1.1 ± 0.1
	20	1.2 ± 0.4	1.0 ± 0.0	1.7 ± 0.1	1.2 ± 0.2	1.1 ± 0.0	1.1 ± 0.0